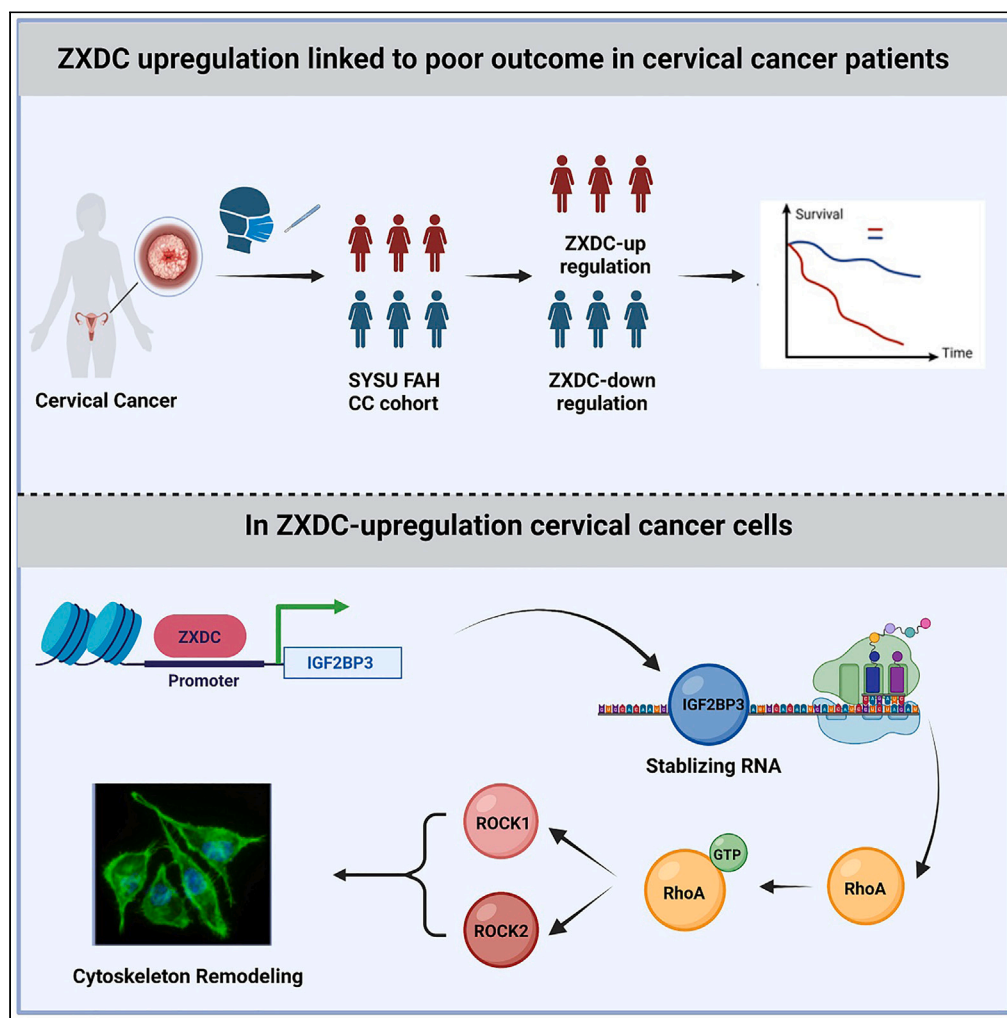


## Article

ZXDC enhances cervical cancer metastasis through *IGF2BP3*-mediated activation of *RhoA/ROCK* signaling

Yifang Mao,  
Xingyu Jiang,  
Peng Guo, ...,  
Tianyi Liang, Yue  
Li, Mian He

liyue1@sysucc.org.cn (Y.L.)  
hemian@mail.sysu.edu.cn  
(M.H.)

**Highlights**

ZXDC can be a negative prognostic marker of cervical cancer patients

ZXDC promotes cervical cancer cell metastasis by regulating cell skeleton remodeling

ZXDC activates *RhoA/ROCK* signaling pathway by regulating *IGF2BP3* expression

## Article

## ZXDC enhances cervical cancer metastasis through IGF2BP3-mediated activation of RhoA/ROCK signaling

Yifang Mao,<sup>1,3</sup> Xingyu Jiang,<sup>2,3</sup> Peng Guo,<sup>1,3</sup> Ying Ouyang,<sup>2</sup> Xiangfu Chen,<sup>2</sup> Meng Xia,<sup>1</sup> Lixin Wu,<sup>1</sup> Zihao Tang,<sup>1</sup> Tianyi Liang,<sup>1</sup> Yue Li,<sup>2,\*</sup> and Mian He<sup>1,4,\*</sup>

## SUMMARY

**Metastasis in cervical cancer (CC) has a significant negative impact on patient survival, highlighting the urgent need for investigation in this area. In this study, we identified significant overexpression of zinc finger, X-linked, duplicated family member C (ZXDC) in CC tissue with metastasis, which correlates with poor outcomes for CC patients. We observed that overexpression of ZXDC promotes, while silencing of ZXDC inhibits the metastasis of CC cells both *in vitro* and *in vivo*. Additionally, our research demonstrated that ZXDC activated RhoA/ROCK signaling pathway, leading to enhanced cytoskeleton remodeling in CC cells. Besides, we found that IGF2BP3 plays an essential role in the activation of ZXDC on the RhoA/ROCK signaling pathway by stabilizing RhoA mRNA. These findings reveal a mechanism whereby ZXDC promotes the cervical cancer metastasis by targeting IGF2BP3/RhoA/ROCK pathway.**

## INTRODUCTION

Cervical cancer is one of the most frequent gynecology malignancies and ranks as the fourth leading cause of cancer death among women globally, with an estimated 604,000 new cases and 342,000 deaths worldwide in 2020.<sup>1</sup> In China alone, there were nearly 110,000 new cases of cervical cancer and about 48,000 deaths, accounting for 18.7% and 15.3% of the global incidence and deaths, respectively.<sup>2</sup> Less developed or developing countries bear approximately 85% of the disease burden of cervical cancer, with a disproportionate impact on low-income areas compared to wealthier regions.<sup>3</sup> Nevertheless, advanced cervical cancer patients have been reported for its poor prognosis, with metastasis being the main negative factor affecting patients' survival.<sup>4,5</sup> Metastasis is often accompanied by increasing complications and the loss of radiotherapy opportunities, emphasizing the need to investigate the mechanism contributing to cervical cancer metastasis.

Enhanced tumor cell motility can have a significant impact on the tumor migration and invasion.<sup>6</sup> Rho GTPases, including RhoA, Rac1, and Cdc42, are a class of small molecular signaling proteins that regulate important cellular functions such as cell adhesion, polarization, proliferation, division, invasion, migration, as well as other important cellular functions.<sup>7</sup> Previous studies have also demonstrated that ROCK kinase, which is activated by RhoA, plays a critical role in intracellular signaling pathways that contributes to cell migration and invasion.<sup>8</sup> The RhoA/ROCK signaling pathway has been shown to be activated in cervical cancer progression.<sup>9–12</sup> Therefore, understanding the molecular mechanisms underlying the RhoA/ROCK pathway in cervical cancer is crucial for the study of tumor occurrence and development.

In our previous study, we revealed that transducing (beta)-like 1X-linked (*TBLR1*) is a potential prognostic marker which has a negative effect on the overall survival in cervical cancer patients.<sup>13</sup> Later transcriptome sequencing results of *TBLR1*-overexpressing and *TBLR1*-knockdown cervical cells identified zinc finger, X-linked, duplicated family member C (ZXDC) as the most significantly differently expressed transcription factor (TF) among all TFs (Figure S1), indicating its potential role in cervical cancer progression. While ZXDC is a transcription factor necessary for the activation of major histocompatibility complex class II genes (MHC II) by *CIITA*, few studies have explored its other functions beyond MHC class II transcription.<sup>14–16</sup> In a separate study, Jon E. Ramsey et al. discovered that ZXDC1, an isoform of ZXDC, may regulate key inflammatory genes and contribute to inflammatory diseases.<sup>17</sup> Therefore, in this study, we hypothesized that ZXDC

<sup>1</sup>Department of Obstetrics and Gynecology, The First Affiliated Hospital of Sun Yat-sen University, Guangzhou 510080, China

<sup>2</sup>Department of Experimental Research, State Key Laboratory of Oncology in South China, Collaborative Innovation Center for Cancer Medicine, Sun Yat-sen University Cancer Center, Guangzhou 510060, China

<sup>3</sup>These authors contributed equally

<sup>4</sup>Lead contact

\*Correspondence: liyue1@sysucc.org.cn (Y.L.), hemian@mail.sysu.edu.cn (M.H.)

<https://doi.org/10.1016/j.isci.2023.107447>



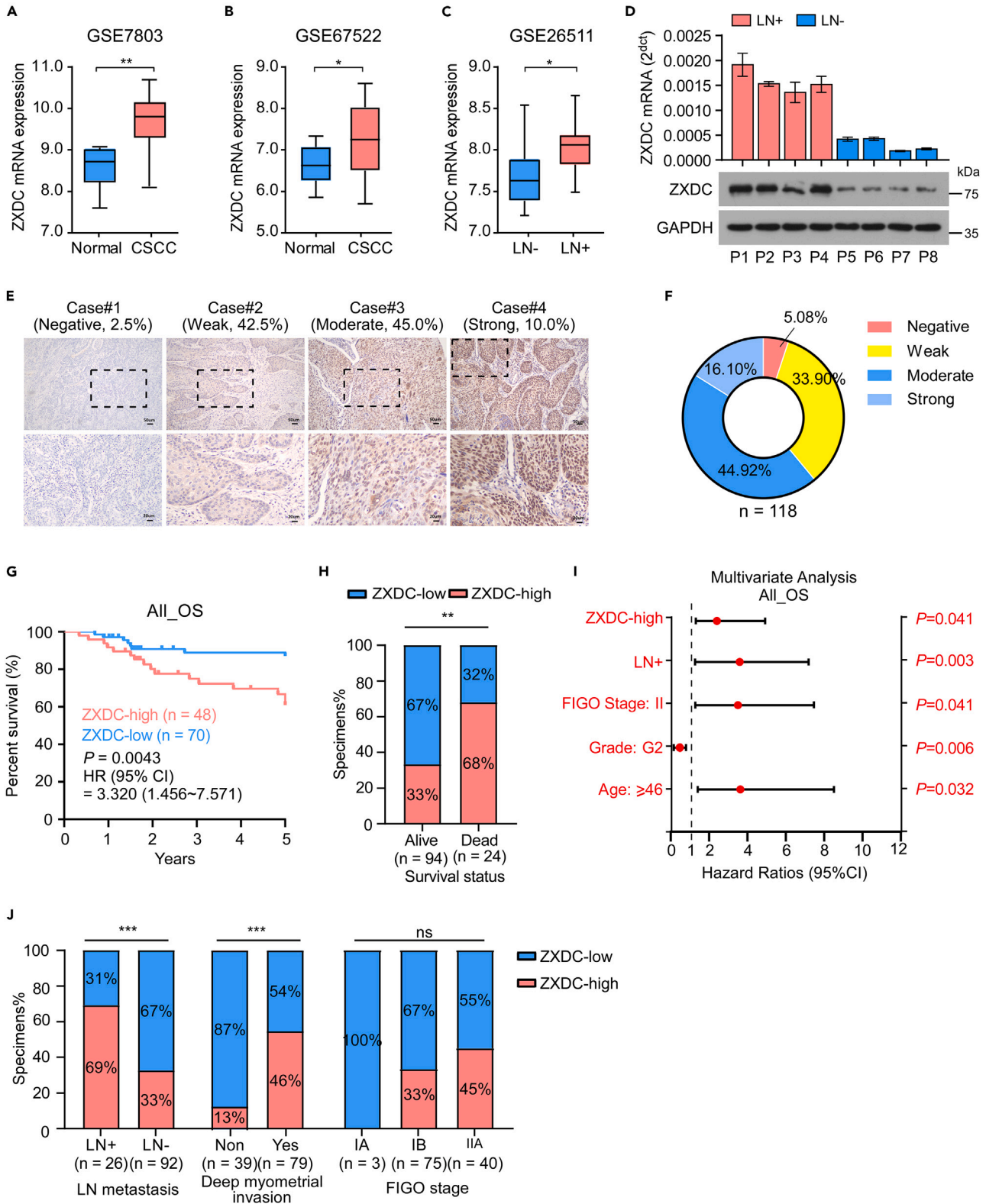


**Figure 1. High ZXDC expression correlated with metastasis and poor prognosis in cervical cancer patients**

(A and B) Different expression level of ZXDC in normal tissues and cervical cancer tissues from GSE7803 (A) and GSE67522 (B) cohorts.  
(C) ZXDC expression significantly correlated with the status of lymph nodes metastasis in GSE26511 cohort. LN-: Negative lymph node metastasis; LN+: Positive lymph node metastasis.  
(D) ZXDC mRNA and protein expression level difference in LN- and LN+ cervical cancer tissues from our center patients. P1–P8: Patient 1–Patient 8. They represent the cervix tissue from different patients.  
(E and F) Representative images (E) and quantification (F) of ZXDC IHC staining in cervical cancer specimens from the patients. Scale bars: 50  $\mu\text{m}$ ; insets: 20  $\mu\text{m}$ .  
(G) Overall survival (OS) analysis in cervical cancer patients stratified by low and high ZXDC expression ( $n = 118$ , log rank test). HR, hazard ratio.  
(H) ZXDC expression significantly correlated with the status of patient survival. Two-sided  $\chi^2$  test were used to evaluate the correlation.  
(I) Multivariate Cox regression analysis to evaluate the significance of the association between high ZXDC expression signature and OS in the presence of other important clinical variables.  
(J) ZXDC expression level correlated with lymph node metastasis, deep myometrial invasion, and FIGO stage.  
Unpaired two-sided Student's  $t$  test was used in (A and B). two-way ANOVA was used in (H and J). \* $p < 0.05$ ; \*\* $p < 0.01$ ; \*\*\* $p < 0.001$ , ns, no significant.

plays a significant role in promoting the metastasis of cervical cancer. Furthermore, to our knowledge, ZXDC has not been extensively studied in cancer, including cervical cancer. Thus, the aim of this study is to investigate the role of ZXDC in cervical cancer progression and elucidate how it promotes cervical cancer metastasis.

In this study, we discovered that ZXDC promotes the progression of cervical cancer and has a significant negative impact on the survival of cervical cancer patients. Mechanistically, ZXDC activates the *RhoA*/ROCK signaling pathway by regulating the transcription of insulin-like growth factor 2 mRNA-binding protein 3 (*IGF2BP3*) mRNA. Additionally, *IGF2BP3* upregulates the *RhoA* and GTP-*RhoA* protein level by stabilizing *RhoA* mRNA, which is essential for the tumor-promoting function of ZXDC in cervical cancer cells. These findings provide important insights into the expression, effects, and mechanism of ZXDC in cervical cancer migration.

**RESULTS****ZXDC correlates with metastasis in cervical cancer**

Based on the upregulation of ZXDC in *TBLR1*-overexpressing cervical cancer cells (Figure S1A), which are known to have a higher metastatic potential than control cells, we hypothesized that ZXDC is involved in regulating cervical cancer metastasis. To further validate this association, we analyzed datasets from the GEO platform and found that ZXDC is highly expressed in cervical cancer tissue compared to normal cervix samples (Figures 1A and 1B). Furthermore, the expression of ZXDC in cervical cancer tissues with positive lymph node (LN) metastasis is significantly higher than in those patients without lymph node metastasis (Figure 1C), providing additional support for the potential role of ZXDC in cervical cancer progression and metastasis.

We examined the distribution of ZXDC mRNA and protein in our center patients with or without lymph node metastasis to validate its expression pattern. We found that expression of ZXDC mRNA and protein is significantly higher in cancer tissues of patients with lymph node metastasis than those without (Figure 1D). To further investigate the clinical relevance of ZXDC protein expression and cervical cancer progression, we performed IHC staining on 118 paraffin-embedded cervical cancer specimens (Table S1). The overall ZXDC staining intensities were divided into four categories: negative (0 score, 5.08%), weak (1 score, 33.90%), moderate (2 score, 44.92%), and strong (3 score, 16.10%) (Figures 1E and 1F). Importantly, higher expression of ZXDC significantly predicted poorer overall survival in cervical cancer patients ( $p = 0.0043$ , HR (95% CI) = 3.320 (1.456–7.571)) (Figure 1G), and there was a higher percentage of higher expressed ZXDC in deceased patients than those alive (Figure 1H).

Furthermore, the multivariate Cox analysis revealed that higher FIGO (The International Federation of Gynecologists and Obstetricians) stage ( $p = 0.041$ ), higher ZXDC expression ( $p = 0.041$ ), positive lymph node metastasis ( $p = 0.003$ ), higher histological grade ( $p = 0.006$ ), and age older than 46 ( $p = 0.032$ ) were independent predictors that affected the overall survival of cervical cancer patients (Figure 1I, Table S2). In addition, higher ZXDC expression was strongly associated with positive LN metastasis, deep myometrial invasion, and FIGO stage (Figure 1J). These findings indicate that ZXDC is linked to the clinical metastasis of cervical cancer and may serve as a valuable prognostic marker for this disease.

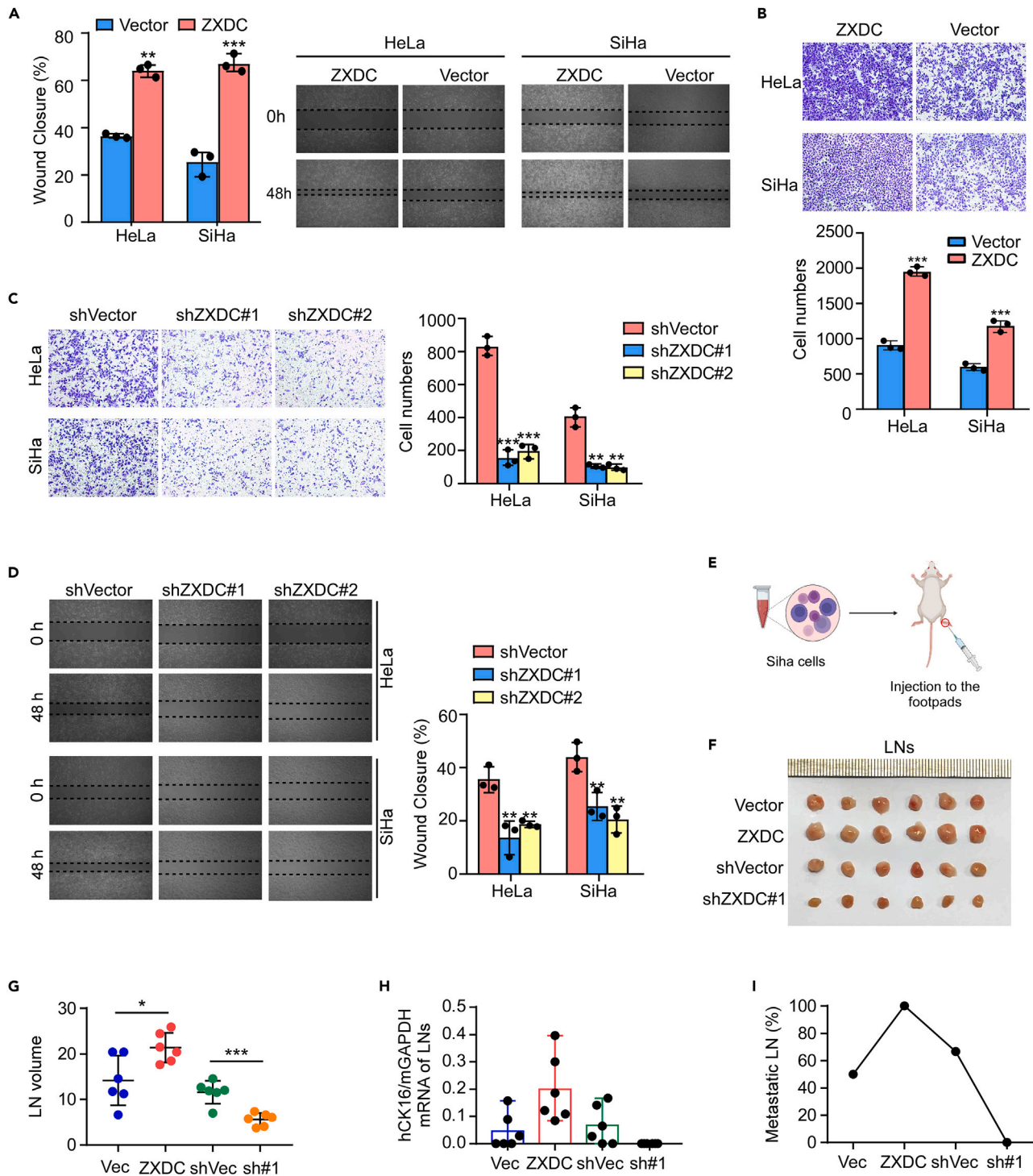


**Figure 2. Zxdc expression level affects the motility of cervical cancer in vivo and in vitro**

(A) Representative images and quantification of invading cells in transwell penetration assays with ZXDC-overexpressing HeLa and SiHa cells.

(B) Representative images and quantification of wound healing assays with ZXDC-overexpressing HeLa and SiHa cells. Images were taken at 0 and 48 h. Percentage of remaining wound area was shown.

(C) Representative images and quantification of invading cells in transwell penetration assays with ZXDC-silencing HeLa and SiHa cells.

(D) Representative images and quantification of wound healing assays with ZXDC-silencing HeLa and SiHa cells. Images were taken at 0 and 48 h. Percentage of remaining wound area was shown.

**Figure 2. Continued**

(E) The construction of xenograft mouse model.

(F) Image of the inguinal lymph nodes (LNs) from each group.

(G) Volumes of the inguinal LNs from each group.

(H) qRT-PCR analysis of human CK16 relative to mouse GAPDH in the LNs from each group. The ratio indicated the proportion of metastatic cells.

(I) The analysis of metastasis LNs ration in each group.

Each error bar in (A and B) and (C and D) represents the mean  $\pm$  SD of three biological replicates. Each error bar in (G and H) represent the mean  $\pm$  SD derived from tumor mouse models (n = 6 mice/group). Two-sided Student's t test was used for all panels. \*p < 0.05; \*\*p < 0.01; \*\*\*p < 0.001.

**ZXDC expression promotes the invasion and motility of cervical cancer cells both *in vitro* and *in vivo***

To investigate the role of ZXDC in cervical cancer metastasis, we generated stable cell lines with either overexpression or knockdown of ZXDC in HeLa and SiHa cervical cancer cells (Figures S2A, S2B, and S4A). Notably, overexpression of ZXDC was associated with more irregular cell shapes and increased number of cell protrusions (Figure S2C), while knockdown of ZXDC resulted in more regular cell shapes and reduced number of cell protrusions (Figure S2D). Furthermore, our results from wound healing assays and the Matrigel-coated transwell assays revealed that upregulation of ZXDC significantly enhanced the migration and invasion ability of cervical cancer cells, while downregulation of ZXDC led to a decrease in these abilities (Figures 2B–2D).

We further investigated the impact of ZXDC on cervical cancer metastasis *in vivo* using popliteal lymph node metastasis model. In this study, we randomly divided mice into four groups (n = 6/group) and injected SiHa-ZXDC and SiHa-shZXDC#1 cells into the right footpads, while SiHa-Vector and SiHa-scramble cells were used as controls (Figure 2E). After 45 days of inoculation, we sacrificed the mice, extracted, and analyzed the primary footpad tumors and popliteal lymph nodes. Notably, higher expression of ZXDC protein promoted LN metastasis, as evidenced by the larger volumes of LNs (Figures 2F and 2G). Furthermore, the relative mRNA ratio of human CK16 to mouse glyceraldehyde 3-phosphate dehydrogenase indicated a higher proportion of colonized tumor cells in LNs (Figures 2H and 2I).

**ZXDC promotes the cytoskeleton remodeling and actin stress fiber formation**

To investigate the mechanism underlying ZXDC-mediated metastasis in cervical cancer cells, we focused on the motility of cancer cells. Previous studies have shown that the movement of the cytoskeleton determines the dynamics and shape of the cells. To visualize the polymerized actin (F-actin), which represents the movement or the remodeling of cytoskeleton, we used phalloidin staining. Interestingly, our results showed that upregulation of ZXDC increased the number of filopodia (Figures 3A, 3B, and S5A), while silencing of ZXDC reduced it (Figures 3D, 3E, S4B, and S5B). Besides, cells with higher expression of ZXDC level had a more irregular distribution of F-actin, indicating more active cytoskeleton remodeling (Figure 3C), while lower expression of ZXDC indicated inactive cytoskeleton remodeling (Figure 3F). Strikingly, we found that overexpression of ZXDC increased the phosphorylation of actin depolymerization factor cofilin to inhibit disassembly, and phosphorylation of the myosin light chain to promote actomyosin contractility (Figure 3G), while silencing of ZXDC reduced it. These observations suggested that ZXDC is involved in the activity of cytoskeleton, which may contribute to cervical cancer cell motility and metastasis.

**ZXDC activates *RhoA/ROCK* signaling pathway through *IGF2BP3***

We conducted further investigations into the underlying mechanism of cytoskeleton remodeling in cervical cancer cells. Previous studies have shown that the *RhoA/ROCK* signal pathway plays a crucial role in regulating cytoskeleton motility and facilitating cell migration.<sup>18,19</sup> Notably, our results revealed that overexpression of ZXDC in cervical cancer cells led to the activation of *RhoA/ROCK* signaling pathway, as evidenced by increases in the protein levels of total-*RhoA*, GTP-bound (active) *RhoA*, *ROCK1*, and *ROCK2*, while silencing of ZXDC reduced levels of these proteins (Figure 4A). Consistently, we also validated this conclusion *in vivo*, as tumors derived from mice transplanted with highly expressed ZXDC SiHa cells exhibited significantly higher levels of *RhoA/ROCK* pathway proteins, further confirming that ZXDC can activate the *RhoA/ROCK* signaling pathway (Figure 4B). Moreover, we observed significantly different levels of *RhoA* mRNA expression between groups (Figure 4C), with higher levels of ZXDC leading to significant upregulation of *RhoA* expression at both the RNA and protein levels.

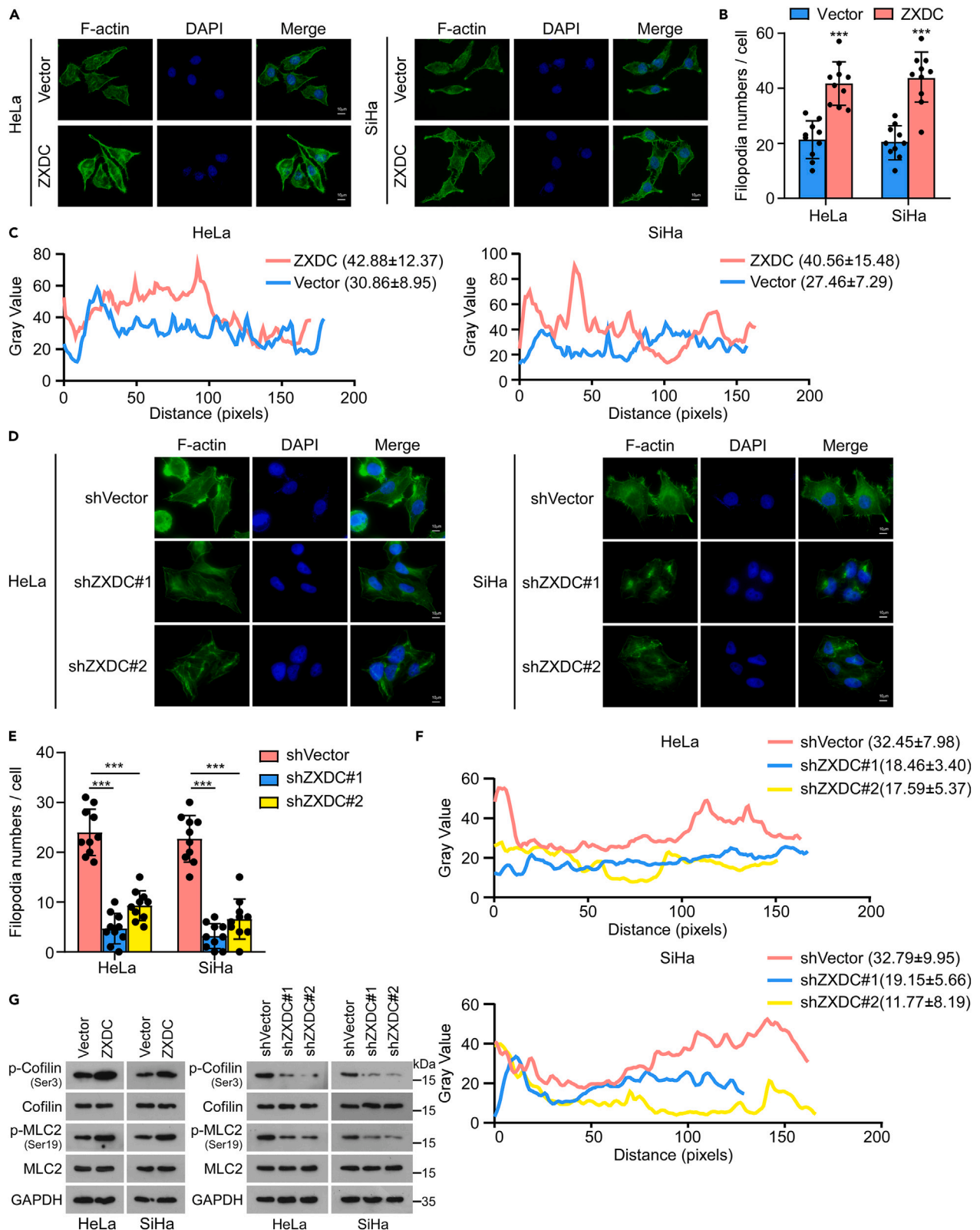


**Figure 3. ZXDC expression level affects the cytoskeleton reorganization in cervical cancer cells**

- (A) F-actin was stained with phalloidin (Green) in HeLa and SiHa cells with ZXDC overexpression.  
(B) The filopodia numbers per cell in HeLa and SiHa cells with ZXDC overexpression.  
(C) The intensity of phalloidin staining was measured used ImageJ in long axis of HeLa and SiHa cells with ZXDC overexpression.  
(D) F-actin was stained with phalloidin (Green) in HeLa and SiHa cells with ZXDC silencing.  
(E) The filopodia numbers per cell in HeLa and SiHa cells with ZXDC silencing.  
(F) The intensity of phalloidin staining was measured used ImageJ in long axis of HeLa and SiHa cells with ZXDC silencing.  
(G) Phosphorylation levels of cofilin and MLC2 were analyzed by Western blot analysis in indicated cells.  
Each error bar in (B and E) represents the mean  $\pm$  SD derived from ten cells. Two-sided Student's t test was used for all panels. \*p < 0.05; \*\*p < 0.01; \*\*\*p < 0.001.

As ZXDC is a transcription factor, we sought to explore the underlying mechanism through which it activates the *RhoA/ROCK* signaling pathway. Surprisingly, when we test the activity of *RhoA* promoter, we found no significant differences between the control group and either ZXDC-overexpressing or ZXDC-silencing groups (Figure 4D), indicating that ZXDC indirectly activates *RhoA/ROCK* signaling pathway. Intriguingly, we discovered that ZXDC can bind to the promoter of *IGF2BP3* (Figure 4E). *IGF2BP3*, also known as *IMP3*, *CT98*, or *VICKZ3*, has been implicated in the development of various cancers.<sup>20</sup> We validated the activity of *IGF2BP3* promoter in different cell groups and found that highly expressed ZXDC group exhibited significantly higher activity (Figure 4F). Furthermore, qPCR analysis revealed that *IGF2BP3* mRNA expression was significantly higher in cells with ZXDC overexpression and lower in cells with ZXDC silencing (Figures S3A and S3B). Chromatin immunoprecipitation (ChIP)-qPCR analysis has shown that ZXDC increased the enrichment of p300, H3K27ac, and RNA polymerase II in HeLa and SiHa cells, indicating that ZXDC can promote the transcription activity of *IGF2BP3* (Figure 4G).

Recently, evidence has shown that *IGF2BP3*, a member of the *IGF2BPs* family, can promote the stability and translation of thousands of potential mRNA targets, thereby globally affecting gene expression output.<sup>21</sup> *IGF2BP3* has also been shown to play an important role in modulating cancer cell fate, including growth, survival, and chemoresistant, by stabilizing encoding mRNA.<sup>22</sup> Thus, in our study, we sought to determine whether *IGF2BP3* was involved in the mechanism by which ZXDC regulates *RhoA* expression. RNA immunoprecipitation assays revealed that *IGF2BP3* specifically binds to *RhoA* mRNA (Figure 4H). To investigate the effect of *IGF2BP3* on the regulation of ZXDC on the *RhoA/ROCK* signaling pathway, we knocked down the *IGF2BP3* in highly expressed ZXDC SiHa cell. Notably, our result showed that SiHa cells with *IGF2BP3* knocked down had the lower expression of *RhoA* mRNA (Figure 4I) and a shorter half-life of *RhoA* mRNA (Figure 4J), indicating that ZXDC controls the stability of *RhoA* mRNA through *IGF2BP3*. As expected, the protein expression level of *RhoA* and the activity of *RhoA/ROCK* signaling pathway were simultaneously reduced in *IGF2BP3*-silencing cells (Figure 4K).

Therefore, the results described previously suggest that ZXDC could potentially activate *RhoA/ROCK* signaling pathway by upregulating *IGF2BP3*.

**IGF2BP3/RhoA/ROCK pathway is essential for ZXDC-induced migration of cervical cancer cells**

To further validate the promotion of cervical cancer cell migration by ZXDC through *IGF2BP3/RhoA/ROCK* pathway, we blocked *RhoA/ROCK* signaling in highly expressed ZXDC SiHa cells by treating them with a ROCK inhibitor called Y-27632. As expected, cervical cancer cells treated with Y-27632 exhibited a more regular shape and fewer protrusions compared to control cells (Figure 5A). Moreover, the results of transwell and wound healing assays revealed that Y-27632 significantly inhibited the migration of ZXDC-overexpressing cervical cancer cells (Figures 5B and 5C). We also performed F-actin staining to validate the role of *RhoA/ROCK* inhibition in ZXDC-mediated cytoskeleton remodeling, and the results showed that Y-27632 significantly decreased cytoskeleton activity in ZXDC-overexpressing SiHa cells (Figure 5D).

**Clinical relevance and study model**

Finally, we investigated the clinical relevance of the ZXDC/*IGF2BP3/RhoA/ROCK* axis in cervical cancer. We observed a significant upregulation of ZXDC, *IGF2BP3*, and GTP-*RhoA* proteins in freshly collected cervical cancer samples from patients with lymph node metastasis compared to those without metastasis (Figure 6A). The expression level relativity curves further supported the clinical relevance of the ZXDC/*IGF2BP3/RhoA* axis in primary tumors (Figure 6).

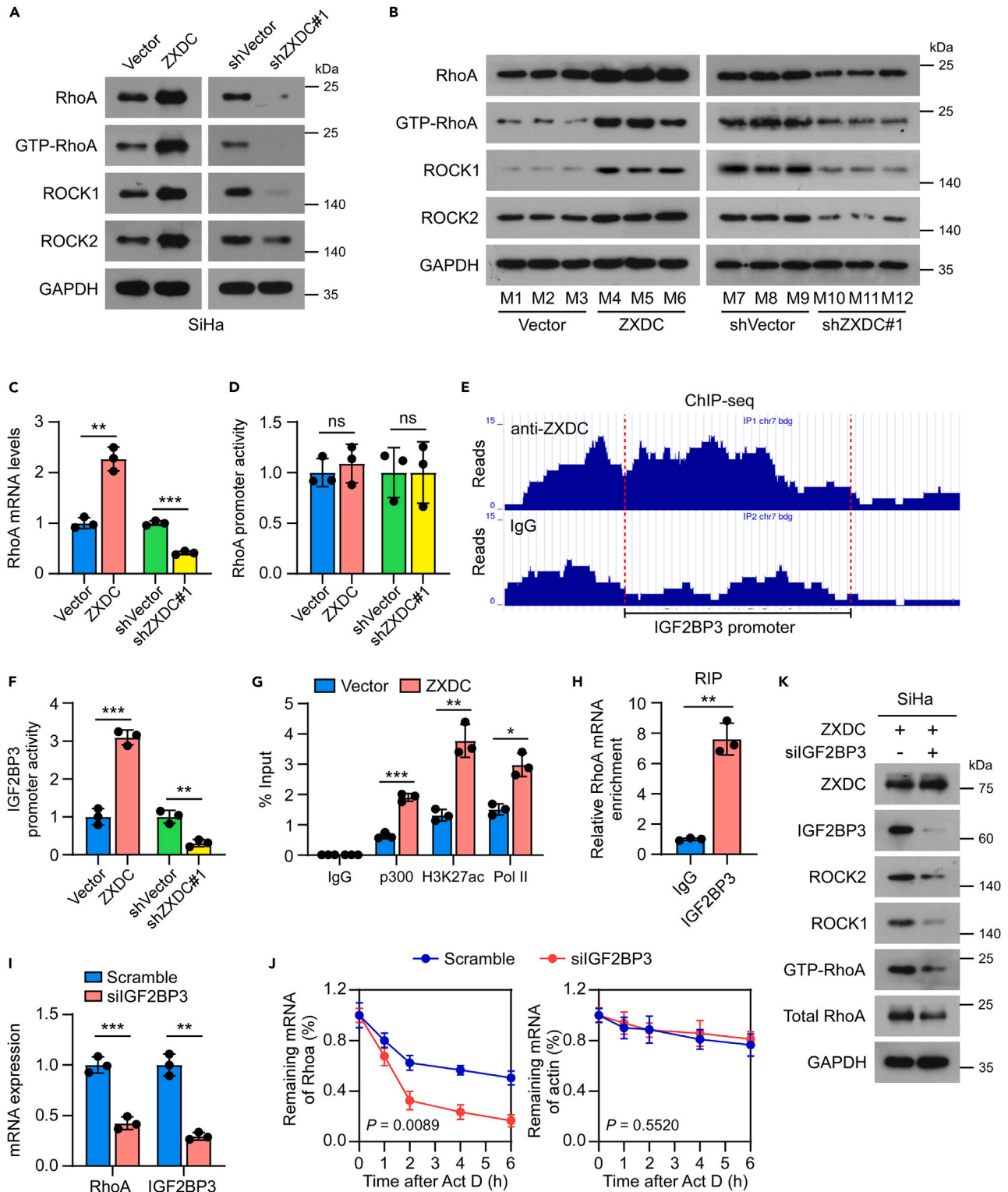


**Figure 4. ZXDC activates RhoA/ROCK signaling pathway through regulating IGF2BP3 expression level**

(A) RhoA/ROCK pathway proteins expression in HeLa and SiHa cells with ZXDC overexpression or silencing.

(B) RhoA/ROCK pathway proteins expression in mice model primary tumor with ZXDC overexpression or silencing. M1–M12: Mouse1–Mouse 12. They represent the tissue from different mouse.

**Figure 4. Continued**

(C) *RhoA* mRNA expression level in SiHa cells with ZXDC overexpression or silencing.

(D) Relative luciferase activities of *RhoA* promoter in SiHa cells with ZXDC overexpressing and silencing.

(E) ChIP assays examined the enrichment of *IGF2BP3* promoter in SiHa cells with ZXDC overexpression or vector.

(F) Relative luciferase activities of *IGF2BP3* promoter in SiHa cells with ZXDC overexpressing and silencing.

(G) The enrichment of p300 acetyltransferase, H3K27ac, and RNA polymerase II (Pol II) on the *OTUD3* promoter in SiHa cells with ZXDC overexpressing and control was determined by ChIP assays.

(H) RIP assays followed by RT-PCR examined the interaction between *IGF2BP3* and *RhoA* mRNAs. *ACTB* was used as a negative control.

(I) *IGF2BP3* and *RhoA/ROCK* pathway mRNA expression level in ZXDC-overexpressing SiHa cells with *IGF2BP3* silencing or not.

(J) ZXDC-overexpressing SiHa cells with or without *IGF2BP3* silencing were treated with Act D (5  $\mu$ g/mL). RNA was isolated at the indicated time points and then subjected to qRT-PCR analysis. The half-lives of mRNAs were traced by calculating the levels relative to the untreated cells.

(K) *IGF2BP3* and *RhoA/ROCK* pathway protein expression level in ZXDC-overexpressing SiHa cells with *IGF2BP3* silencing or not.

Each error bar in (C and D) and (F–I) represents the mean  $\pm$  SD derived from three biological replicates. Two-sided Student's t test was used for all panels. \* $p < 0.05$ ; \*\* $p < 0.01$ ; \*\*\* $p < 0.001$ ; ns, no significance.

In conclusion, our study demonstrates that ZXDC promotes cell cytoskeleton remodeling and migration of cervical cancer cells by activating the *RhoA/ROCK* signaling pathway through *IGF2BP3* (Figure 6). This finding shed light on the underlying mechanism of ZXDC in cancer metastasis and suggests that ZXDC may serve as a promising prognostic marker.

**DISCUSSION**

Metastasis and limited treatment options pose significant challenges for oncologists in advanced cervical cancer. Our study has shown that high expression of ZXDC protein is associated with poor prognosis and increased metastasis in early-stage cervical cancer. Specifically, our results indicate that higher expression of ZXDC can promote the metastasis of cervical cancer cells, suggesting that ZXDC may be a valuable biomarker for the diagnosis and prognosis in cervical cancer patients. However, there are limited studies on the role of ZXDC in cancer progression, especially in cervical cancer.

Yasuhiro Kuramitsu et al.<sup>23</sup> evaluated the expression of ZXDC in malignant invasive cells and control cells, and found that its expression in malignant invasive cells was lower. They suggested that the reason is that ZXDC protein can activate the transcription of MHC molecules to mediate tumor immunity, indicating that ZXDC may have a tumor suppressor effect, but its function and mechanism were not explored. In contrast, Halkin et al. analyzed the downstream proteins of ZXDC and found that ZXDC, as a transcription factor, can promote the expression of genes involved in cell cycle, cell proliferation, and differentiation.<sup>24</sup> Our study seems to contradict Yasuhiro's findings, but Halkin's results suggest that ZXDC can regulate the transcription of a series of genes. Based on this evidence, ZXDC protein may promote the progression of cervical cancer cells in patients. As such, it is of great value to further investigate the mechanism of ZXDC, which may provide new clues for potential targeting of ZXDC.

Metastasis is a multi-step process that involves the escape of cancer cells from the primary tumor to spread and invade distant tissues. Tumor cell migration and invasion representing a fundamental property are necessary for cancer invasion and ultimately metastatic dissemination.<sup>25</sup> Previous studies have shown that cancer cell migration is regulated by a rearrangement of the cytoskeleton, specifically by cycles of polymerization and depolymerization of actin filaments, which affects the cell morphology.<sup>26,27</sup> Therefore, cytoskeleton remodeling can be observed during the migration of cancer cells, along with changes in cell morphology.<sup>19A</sup> In our study, we found that the expression of ZXDC protein can affect the cell morphology of cervical cancer cells. Moreover, F-actin staining showed that ZXDC can regulate cytoskeleton remodeling.

Rho GTPases are frequently activated in human cancers and play critical roles in invasion and metastasis of cancer cells by regulating cell motility and the organization of actin cytoskeleton dynamics. *In vitro* experiments conducted by Xiaojun Liu et al. demonstrated that *RhoA* overexpression together with *ROCK1* and *ROCK2* supports the spreading and migration of HeLa cells, indicating a higher metastatic potential of cancer cells.<sup>8A</sup> Our study further supports this finding and suggests that understanding the regulation of *RhoA* activity could provide new targetable vulnerabilities of tumors. In our experiments, we found that ZXDC regulates the cytoskeleton remodeling through the activation of *RhoA/ROCK* signaling. Inhibition of *RhoA/ROCK* reduced the promotion of migration by cervical cancer cells mediated by ZXDC. Notably, our study revealed that ZXDC, as a transcription factor, does not regulate the transcription of *RhoA*

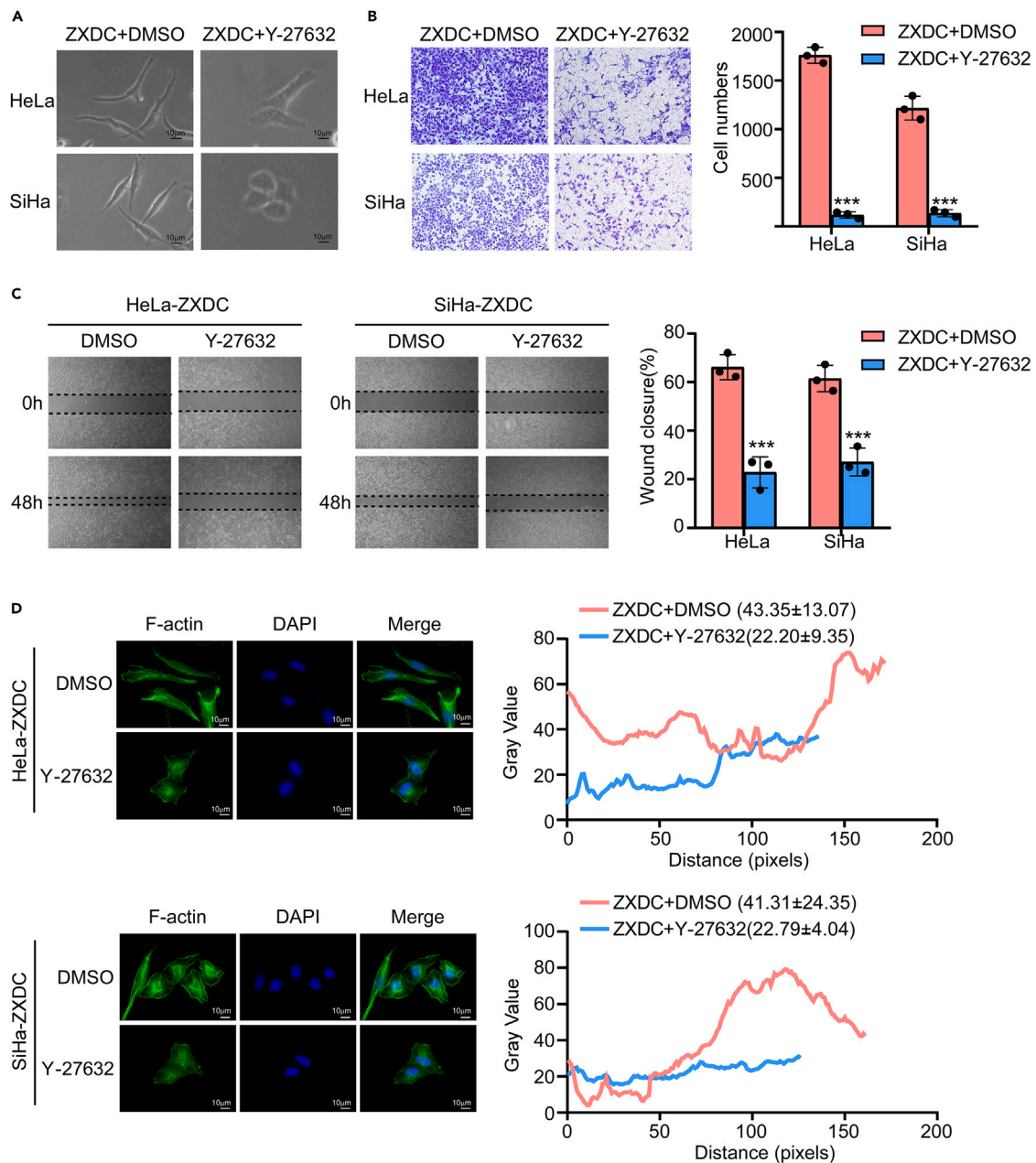


**Figure 5. ZXDC promotes the metastasis of cervical cancer cells via IGF2BP3/RhoA/ROCK pathway**

(A) The morphology was pictured used a light microscope in ZXDC-overexpressing HeLa and SiHa cells with ROCK inhibitor (Y-27632). DMSO was used as a negative control.

(B) Representative images and quantification of invading cells in transwell penetration assays in ZXDC-overexpressing HeLa and SiHa cells with Y-27632.

(C) Representative images and quantification of wound healing assays in ZXDC-overexpressing HeLa and SiHa cells with Y-27632. Images were taken at 0 and 48 h. Percentage of remaining wound area was shown.

(D) F-actin was stained with phalloidin (Green) in ZXDC-overexpressing HeLa and SiHa cells with Y-27632.

Each error bar in (B and C) represents the mean  $\pm$  SD derived from three biological replicates. Two-sided Student's t test was used for all panels. \* $p < 0.05$ ; \*\* $p < 0.01$ ; \*\*\* $p < 0.001$ .

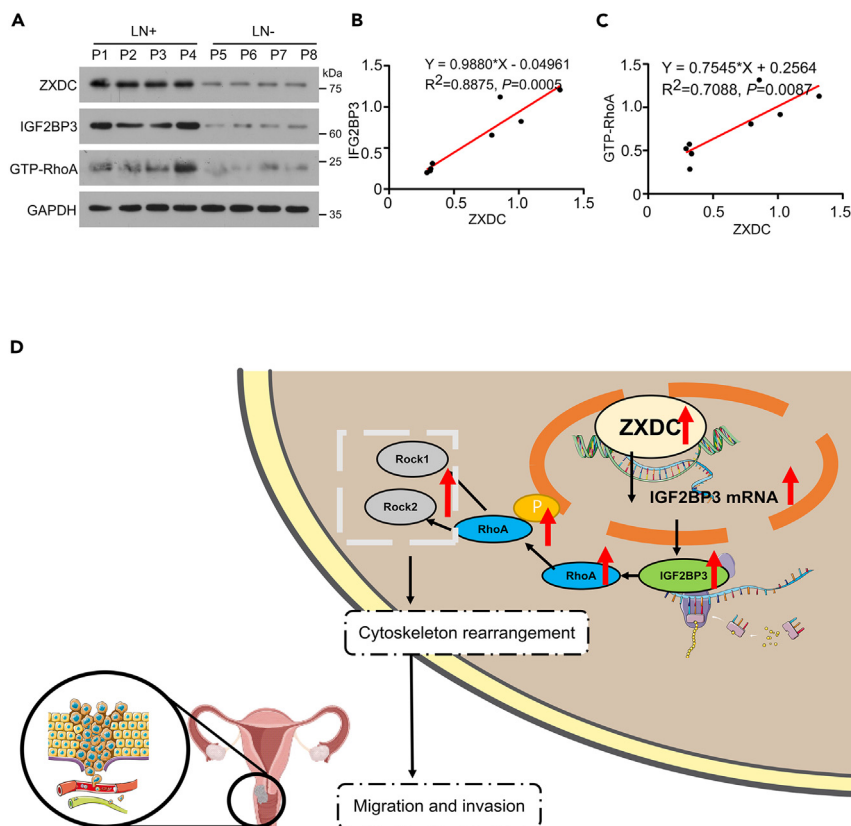


**Figure 6. Clinical relevance of ZXDC and IGF2BP3/RhoA/ROCK signaling pathway**

(A) ZXDC, IGF2BP3, and GTP-RhoA protein expression level in primary tumor tissues from patients with or without lymph nodes metastasis.

(B and C) Correlation analysis of ZXDC, IGF2BP3, and GTP-RhoA in clinical tumor tissues.

(D) Study model: ZXDC activates RhoA/ROCK signaling pathway via regulating IGF2BP3 expression level, leading to the cervical cancer cells metastasis.

gene mRNA, but it can promote the protein expression of RhoA and GTP-RhoA. Our ChIP sequencing (ChIP-seq) results seem to support this conclusion.

IGF2BP3 belongs to the insulin-like growth factor 2 mRNA-binding protein family and is expressed primarily during embryogenesis and is almost absent in normal adult tissues; however, it is often re-expressed in cancer and is known to be involved in the regulation of RNA transport, translation, and conversion by binding to the coding regions of targeted mRNAs. Our ChIP-seq analysis showed that ZXDC binds to the promoter of IGF2BP3 and promotes its transcription, leading to upregulation of IGF2BP3 protein expression. Numerous studies have demonstrated the essential role of IGF2BP3 in different cancers, such as colon cancer, bladder cancer, and oral cancer. Previous studies have shown that IGF2BP3, as a reader of m6A and a posttranscriptional regulator of gene expression, is closely related to the proliferation, migration, and chemotherapy resistance of tumor cells.<sup>28,29</sup> Moreover, Fan Ren et al.<sup>30</sup> studied in zebrafish and proposed that depletion of maternal IGF2BP3 would destabilize the maternal mRNA prior to the maternal-to-zygotic transition, resulting in abnormal cytoskeleton organization. Besides, Clarissa C Pasilliao et al.<sup>6</sup> showed that IGF2BP3 facilitates the progression pancreatic ductal adenocarcinoma progression by modulating the levels of proteins involved in cytoskeletal organization, including GTP-RhoA protein. Our study suggests that IGF2BP3 can promote the transcription of RhoA by stabilizing RhoA mRNA, which can fully activate downstream RhoA signaling and regulate the remodeling of cell cytoskeleton, promoting cancer progression.

In summary, our study indicates that ZXDC can activate RhoA/ROCK signaling pathway through regulating the transcription of IGF2BP3, which significantly promotes the metastasis of cervical cancer. A deeper

understanding of the precise role of ZXDC in cervical cancer progression, as well as the mechanism by which it operates, would increase our knowledge of the biological basis of cervical cancer metastasis.

### Limitations of the study

Although our study provides important insights into the role of ZXDC in cervical cancer metastasis, there are several limitations that should be acknowledged. One limitation is that we only used two short hairpin RNA (shRNA) against ZXDC, which may increase the risk of off-target effects. Similarly, several experiments used just one shRNA, which limits our ability to draw robust conclusions. In the future, maybe we will conduct rescue experiment or validate our conclusion from other aspect. Second limitation is that several other genes were also found in the ChIP-seq analysis, which was not investigated in our study. Whether other downstream genes contribute to the malignant phenotype of ZXDC in cervical cancer remained to be further determined. Besides, we proposed that ZXDC can activate *RhoA/ROCK* signaling pathway through regulating the transcription of *IGF2BP3*; however, the mechanism was not fully clarified. Finally, we did not perform enough *in vitro* metastasis function experiment to better validate our conclusion, like 3D invasion assay. In the future, we can explore more metastasis function-relating experiments to better confirm the role of ZXDC on cervical cancer metastasis. While there are some limitations of our experimental designs, we do suggest that further research is needed to confirm and extend our results.

### STAR★METHODS

Detailed methods are provided in the online version of this paper and include the following:

- KEY RESOURCES TABLE
- RESOURCE AVAILABILITY
  - Lead contact
  - Materials availability
  - Data and code availability
- EXPERIMENT MODEL AND STUDY PARTICIPANT DETAILS
  - Cell lines
  - Patients and tissues
  - Xenograft mouse model
- METHOD DETAILS
  - Bioinformatic analysis
  - Immunohistochemistry (IHC)
  - RNA isolation and quantitative real-time PCR (qRT-PCR)
  - Western blot analysis
  - Immunofluorescence staining of F-actin and filopodia counting
  - F-actin quantification
  - Luciferase reporter assays
  - *RhoA* activity assay
  - RNA IP (RIP) assays
  - DNA constructs and establishment of stable cell lines
  - Chromatin immunoprecipitation (ChIP) assay
  - Wound healing assay
  - Transwell migration assay
  - Primers and oligonucleotides
- QUANTIFICATION AND STATISTICAL ANALYSIS

### SUPPLEMENTAL INFORMATION

Supplemental information can be found online at <https://doi.org/10.1016/j.isci.2023.107447>.

### ACKNOWLEDGMENTS

This study was funded by the National Natural Science Foundation of China (81872118, 82203113), Guangzhou Science and Technology Project (no.202002030003), China Postdoctoral Science Foundation (2022M723623).

## AUTHOR CONTRIBUTIONS

Conception and design: M.H. and Y.L. Development of methodology: Y.M., X.J., and P.G. Analysis and interpretation of data (e.g., statistical analysis, biostatistics, computational analysis): Y.M., X.J., P.G., Y.O., X.C., M.X., L.W., Z.T., and T.L. Writing, review, and/or revision of the manuscript: M.H. and Y.L. Study supervision: M.H. and Y.L.

## DECLARATION OF INTERESTS

The authors declare no conflict of interest.

Received: January 19, 2023

Revised: April 17, 2023

Accepted: July 18, 2023

Published: July 20, 2023

## REFERENCES

- Sung, H., Ferlay, J., Siegel, R.L., Laversanne, M., Soerjomataram, I., Jemal, A., and Bray, F. (2021). Global Cancer Statistics 2020: GLOBOCAN Estimates of Incidence and Mortality Worldwide for 36 Cancers in 185 Countries. *CA. Cancer J. Clin.* 71, 209–249. <https://doi.org/10.3322/caac.21660>.
- Zou, Z., Fairley, C.K., Ong, J.J., Hocking, J., Canfell, K., Ma, X., Chow, E.P.F., Xu, X., Zhang, L., and Zhuang, G. (2020). Domestic HPV vaccine price and economic returns for cervical cancer prevention in China: a cost-effectiveness analysis. *Lancet Global Health* 8, e1335–e1344. [https://doi.org/10.1016/S2214-109X\(20\)30277-1](https://doi.org/10.1016/S2214-109X(20)30277-1).
- Yang, S., Sun, Y., Jiang, D., Wang, J., Dang, E., Li, Z., Zhou, J., Lu, Y., Shi, J., Tao, L., et al. (2021). MiR-362 suppresses cervical cancer progression via directly targeting BAP31 and activating TGF $\beta$ /Smad pathway. *Cancer Med.* 10, 305–316. <https://doi.org/10.1002/cam4.3601>.
- Deng, M., Cai, X., Long, L., Xie, L., Ma, H., Zhou, Y., Liu, S., and Zeng, C. (2019). CD36 promotes the epithelial-mesenchymal transition and metastasis in cervical cancer by interacting with TGF- $\beta$ . *J. Transl. Med.* 17, 352. <https://doi.org/10.1186/s12967-019-2098-6>.
- Feng, S., Liu, W., et al. (2019). LncRNA-CTS promotes metastasis and epithelial-to-mesenchymal transition through regulating miR-505/ZEB2 axis in cervical cancer. *Cancer Lett* 465, 105–117. <https://doi.org/10.1016/j.canlet.2019.09.002>.
- Pasilliao, C.C., Chang, C.W.A., Sutherland, B.W., Valdez, S.M., Schaeffer, D., Yapp, D.T., and Ng, S.S.W. (2015). The involvement of insulin-like growth factor 2 binding protein 3 (IMP3) in pancreatic cancer cell migration, invasion, and adhesion. *BMC Cancer* 15, 266. <https://doi.org/10.1186/s12885-015-1251-8>.
- Sahai, E., and Marshall, C.J. (2002). RHO-GTPases and cancer. *Nat. Rev. Cancer* 2, 133–142. <https://doi.org/10.1038/nrc725>.
- Barcelo, J., Samain, R., and Sanz-Moreno, V. (2023). Preclinical to clinical utility of ROCK inhibitors in cancer. *Trends Cancer* 9, 250–263. <https://doi.org/10.1016/j.trecan.2022.12.001>.
- Liu, X., Chen, D., and Liu, G. (2014). Overexpression of RhoA promotes the proliferation and migration of cervical cancer cells. *Biosci. Biotech. Biochem.* 78, 1895–1901. <https://doi.org/10.1080/09168451.2014.943650>.
- Zubor, P., Dankova, Z., Kolkova, Z., Holubekova, V., Brany, D., Mersakova, S., Samec, M., et al. (2020). Rho GTPases in Gynecologic Cancers: In-Depth Analysis toward the Paradigm Change from Reactive to Predictive, Preventive, and Personalized Medical Approach Benefiting the Patient and Healthcare. *Cancers (Basel)* 12. <https://doi.org/10.3390/cancers12051292>.
- Li, X., Li, D., and Ma, R. (2022). ALW-II-41-27, an EphA2 inhibitor, inhibits proliferation, migration and invasion of cervical cancer cells via inhibition of the RhoA/ROCK pathway. *Oncol. Lett.* 23, 129. <https://doi.org/10.3892/ol.2022.13249>.
- Yuan, B., Cui, J., Wang, W., and Deng, K. (2016). G $\alpha$ 12/13 signaling promotes cervical cancer invasion through the RhoA/ROCK-JNK signaling axis. *Biochemical and biophysical research communications* 473, 1240–1246. <https://doi.org/10.1016/j.bbrc.2016.04.048>.
- Wang, J., Ou, J., Guo, Y., Dai, T., Li, X., Liu, J., Xia, M., Liu, L., and He, M. (2014). TBLR1 is a novel prognostic marker and promotes epithelial-mesenchymal transition in cervical cancer. *Br. J. Cancer* 111, 112–124. <https://doi.org/10.1038/bjc.2014.278>.
- Al-Kandari, W., Jambunathan, S., Navalgund, V., Koeni, R., Freer, M., Parimi, N., Mudhasani, R., and Fontes, J.D. (2007). ZXDC, a novel zinc finger protein that binds CIITA and activates MHC gene transcription. *Mol. Immunol.* 44, 311–321. <https://doi.org/10.1016/j.molimm.2006.02.029>.
- Jambunathan, S., and Fontes, J.D. (2007). Sumoylation of the zinc finger protein ZXDC enhances the function of its transcriptional activation domain. *Biol. Chem.* 388, 965–972. <https://doi.org/10.1515/bc.2007.106>.
- Al-Kandari, W., Koeni, R., Navalgund, V., Aleksandrova, A., Jambunathan, S., and Fontes, J.D. (2007). The zinc finger proteins ZXDA and ZXDC form a complex that binds CIITA and regulates MHC II gene transcription. *Journal of molecular biology* 369, 1175–1187. <https://doi.org/10.1016/j.jmb.2007.04.033>.
- Ramsey, J.E., and Fontes, J.D. (2013). The zinc finger transcription factor ZXDC activates CCL2 gene expression by opposing BCL6-mediated repression. *Mol. Immunol.* 56, 768–780. <https://doi.org/10.1016/j.molimm.2013.07.001>.
- Zhou, Q., Gensch, C., Liao, J.K., and Mitchison, T.J. (1997). Actin dynamics in vivo. *Curr. Opin. Cell Biol.* 9, 167–173. [https://doi.org/10.1016/S0955-0674\(97\)80152-4](https://doi.org/10.1016/S0955-0674(97)80152-4).
- Zhou, Q., Gensch, C., and Liao, J.K. (2011). Rho-associated coiled-coil-forming kinases (ROCKs): potential targets for the treatment of atherosclerosis and vascular disease. *Trends in pharmacological sciences* 32, 167–173. <https://doi.org/10.1016/j.tips.2010.12.006>.
- Wang, C., Kong, F., Ma, J., Miao, J., Su, P., Yang, H., Li, Q., and Ma, X. (2022). IGF2BP3 enhances the mRNA stability of E2F3 by interacting with LINC00958 to promote endometrial carcinoma progression. *Cell Death Discov.* 8, 279. <https://doi.org/10.1038/s41420-022-01045-x>.
- Huang, H., Weng, H., Sun, W., Qin, X., Shi, H., Wu, H., Zhao, B.S., Mesquita, A., Liu, C., Yuan, C.L., et al. (2018). Recognition of RNA N(6)-methyladenosine by IGF2BP proteins enhances mRNA stability and translation. *Nat. Cell Biol.* 20, 285–295. <https://doi.org/10.1038/s41556-018-0045-z>.
- Lederer, M., Bley, N., Schleifer, C., and Hüttelmaier, S. (2014). The role of the oncofetal IGF2 mRNA-binding protein 3 (IGF2BP3) in cancer. *Semin. Cancer Biol.* 29, 3–12. <https://doi.org/10.1016/j.semcancer.2014.07.006>.
- Kuramitsu, Y., Hayashi, E., Okada, F., Tanaka, T., Zhang, X., Ueyama, Y., and Nakamura, K. (2010). Proteomic analysis for nuclear proteins related to tumour malignant progression: a

comparative proteomic study between malignant progressive cells and regressive cells. *Anticancer Res.* 30, 2093–2099.

24. Halkin, O.V., and Minchenko, O.H. (2010). [Changes in genes expression caused by overexpression of the transcription factor ZXDC in embryonic kidney cell line HEK293]. *Ukr. Biokhim. Zh.* (1999) 82, 100–107.
25. Tabdanov, E.D., Puram, V.V., Win, Z., Alamgir, A., Alford, P.W., and Provenzano, P.P. (2018). Bimodal sensing of guidance cues in mechanically distinct microenvironments. *Nat. Commun.* 9, 4891. <https://doi.org/10.1038/s41467-018-07290-y>.
26. Chamlali, M., Kouba, S., Rodat-Despoix, L., Todesca, L.M., Pethö, Z., Schwab, A., and Ouadid-Ahidouch, H. (2021). Orai3 Calcium Channel Regulates Breast Cancer Cell Migration through Calcium-Dependent and -Independent Mechanisms. *Cells* 10. <https://doi.org/10.3390/cells10123487>.
27. Vautrin-Glabik, A., Botia, B., Kischel, P., Ouadid-Ahidouch, H., and Rodat-Despoix, L. (2018). IP(3)R3 silencing induced actin cytoskeletal reorganization through ARHGAP18/RhoA/mDia1/FAK pathway in breast cancer cell lines. *Biochimica et biophysica acta. Molecular cell research* 1865, 945–958. <https://doi.org/10.1016/j.bbamcr.2018.04.002>.
28. Yang, Z., Wang, T., Wu, D., Min, Z., Tan, J., and Yu, B. (2020). RNA N6-methyladenosine reader IGF2BP3 regulates cell cycle and angiogenesis in colon cancer. *J. Exp. Clin. Cancer Res.* 39, 203. <https://doi.org/10.1186/s13046-020-01714-8>.
29. Huang, W., Li, Y., Zhang, C., Zha, H., Zhou, X., Fu, B., Guo, J., and Wang, G. (2020). IGF2BP3 facilitates cell proliferation and tumorigenesis via modulation of JAK/STAT signalling pathway in human bladder cancer. *J. Cell Mol. Med.* 24, 13949–13960. <https://doi.org/10.1111/jcmm.16003>.
30. Ren, F., Lin, Q., Gong, G., Du, X., Dan, H., Qin, W., Miao, R., Xiong, Y., Xiao, R., Li, X., et al. (2020). Igf2bp3 maintains maternal RNA stability and ensures early embryo development in zebrafish. *Commun. Biol.* 3, 94. <https://doi.org/10.1038/s42003-020-0827-2>.
31. Zhai, Y., Kuick, R., Nan, B., Ota, I., Weiss, S.J., Trimble, C.L., Fearon, E.R., and Cho, K.R. (2007). Gene expression analysis of preinvasive and invasive cervical squamous cell carcinomas identifies HOXC10 as a key mediator of invasion. *Cancer Res.* 67, 10163–10172. <https://doi.org/10.1158/0008-5472.Can-07-2056>.
32. Saha, S.S., Chowdhury, R.R., Mondal, N.R., Roy, S., and Sengupta, S. (2017). Expression signatures of HOX cluster genes in cervical cancer pathogenesis: Impact of human papillomavirus type 16 oncoprotein E7. *Oncotarget* 8, 36591–36602. <https://doi.org/10.18632/oncotarget.16619>.
33. Noordhuis, M.G., Fehrmann, R.S.N., Wisman, G.B.A., Nijhuis, E.R., van Zanden, J.J., Moerland, P.D., Ver Loren van Themaat, E., Volders, H.H., Kok, M., ten Hoor, K.A., et al. (2011). Involvement of the TGF-beta and beta-catenin pathways in pelvic lymph node metastasis in early-stage cervical cancer. *Clin. Cancer Res.* 17, 1317–1330. <https://doi.org/10.1158/1078-0432.Ccr-10-2320>.
34. Meng, H., Yang, S., Li, Z., Xia, T., Chen, J., Ji, Z., Zhang, H., Wang, X., Lin, S., Huang, C., et al. (2011). Aspect ratio determines the quantity of mesoporous silica nanoparticle uptake by a small GTPase-dependent macropinocytosis mechanism. *ACS Nano* 5, 4434–4447. <https://doi.org/10.1021/nn103344k>.
35. Al Absi, A., Wurzer, H., Guerin, C., Hoffmann, C., Moreau, F., Mao, X., Brown-Clay, J., Petrolli, R., Casellas, C.P., Dieterle, M., et al. (2018). Actin Cytoskeleton Remodeling Drives Breast Cancer Cell Escape from Natural Killer-Mediated Cytotoxicity. *Cancer Res.* 78, 5631–5643. <https://doi.org/10.1158/0008-5472.Can-18-0441>.

STAR★METHODS

KEY RESOURCES TABLE

REAGENT or RESOURCE	SOURCE	IDENTIFIER
<b>Antibodies</b>		
Rabbit polyclonal anti-ZXDC	Proteintech	Cat#20530-1-AP, RRID: AB_10694823
Rabbit monoclonal anti-RhoA	Cell Signaling Technology	Cat#2117, RRID: AB_10693922
Rabbit monoclonal anti-ROCK1	Cell Signaling Technology	Cat#4035, RRID: AB_2238679
Rabbit polyclonal anti-IGF2BP3	Proteintech	Cat#14642-1-AP, RRID: AB_2122782
Rabbit monoclonal anti-p-Cofilin S3	Cell Signaling Technology	Cat#3313, RRID:AB_2080597
Rabbit monoclonal anti-Cofilin	Cell Signaling Technology	Cat#5175, RRID: AB_10622000
Rabbit polyclonal anti-p-MLC2 S19	Cell Signaling Technology	Cat#3671, RRID: AB_330248
Rabbit monoclonal anti- MLC2	Cell Signaling Technology	Cat#8505, RRID: AB_2728760
Rabbit polyclonal anti-ROCK2	Cell Signaling Technology	Cat#8236, RRID: AB_10829468
Rabbit monoclonal GAPDH (D16H11)	Cell Signaling Technology	Cat#5174, RRID: AB_10622025
Mouse monoclonal anti-Tubulin (DM1A)	Sigma-Aldrich	Cat#T9026; RRID: AB_477593
<b>Bacterial and virus strains</b>		
E. Coli strain DH5 $\alpha$	TIANGEN	Cat#CB101-02
E. Coli strain Stbl3	AngYuBio	Cat#G6009
<b>Biological samples</b>		
Human cervical cancer tissue	The first affiliated hospital of Sun Yat-sen University	N/A
<b>Chemicals, peptides, and recombinant proteins</b>		
Actinomycin D	Sigma-Aldrich	Cat#A9415
Alexa Fluor® 488 Phalloidin	Cell Signaling Technology	Cat#8878
<b>Critical commercial assays</b>		
Dual-Luciferase Reporter Assay Kit	Promega	Cat#E1910
Active Rho Detection Kit	Cell Signaling Technology	Cat#8820
SimpleChIP® Enzymatic Chromatin IP Kit (Agarose Beads)	Cell Signaling Technology	Cat#9002
<b>Deposited data</b>		
Chip-seq of ZXDC in cervical cancer cells	NCBI Sequence Read Archive (SRA) database	PRJNA978350
ZXDC is highest expressed transcription factor on TBLR1-overexpressed HeLa cells	NCBI Gene Expression Omnibus (GEO) database	GSE234087
<b>Experimental models: Cell lines</b>		
HeLa cell	ATCC	N/A
SiHa cell	ATCC	N/A
<b>Experimental models: Organisms/strains</b>		
SCID	GemPharmatech	N/A
<b>Oligonucleotides</b>		
hGAPDH-F-primer: GTCTCCTGACTTCAACAGCG-	This paper	N/A
hGAPDH-R-primer: ACCACCCTGTTGCTGTAGCCAA	This paper	N/A
hZXDC-F-Primer: AGGATGTGGGTGCTCCGAAAAG	This paper	N/A
hZXDC-R-Primer: CGGAGCTTCTAGCTGAGGTAAG	This paper	N/A

(Continued on next page)

**Continued**

REAGENT or RESOURCE	SOURCE	IDENTIFIER
hKRT17-F-Primer: ATCCTGCTGGATGTGAAGACGC	This paper	N/A
hKRT17-R-Primer: TCCACAATGGTACGCACCTGAC	This paper	N/A
hRHOA-F-Primer: TCTGTCCCAACGTGCCCATCAT	This paper	N/A
hRHOA-R-Primer: CTGCCTTCTTCAGGTTTCACCG	This paper	N/A
hACTB-F-Primer: CACCATTGGCAATGAGCGGTTTC	This paper	N/A
hACTB-R-Primer: AGGTCTTTGCGGATGTCCACGT	This paper	N/A
hIGF2BP3-F-primer: TCGTGACCAGACACCTGATGAG	This paper	N/A
hIGF2BP3-R-primer: GGTGCTGCTTTACCTGAGTCAG	This paper	N/A
mGAPDH-F-Primer: CATCACTGCCACCCAGAAGACTG	This paper	N/A
mGAPDH-R-Primer: ATGCCAGTGAGCTTCCCGTTCAG	This paper	N/A
ZXDC promoter region-F-Primer: GGACGACAAACCTGAAGC	This paper	N/A
ZXDC promoter region-R-Primer: CTGGGCGATAGAGGGAGA	This paper	N/A
non-Promoter region-F-Primer: GAAGGCTGTGGGAGATGA	This paper	N/A
non-Promoter region-R-Primer: CCGATGACCATTAGAGGG	This paper	N/A
ZXDC-shRNA#1: GCAGTCTGTACATCACTCTA TTCAAGAGATAGAGTGAATGTACAGACTGC	This paper	N/A
shRNA#2: TGACGATACCCGGAGGTTTACTTC AAGAGAGTAAACCTCCGGTCATCGTCA	This paper	N/A
<b>Recombinant DNA</b>		
pLVX-puro-ZXDC-3Flag	This paper	N/A
<b>Software and algorithms</b>		
SPSS Statistics version 19.0	IBM	<a href="https://www.ibm.com/cn-zh/products/spss-statistics">https://www.ibm.com/cn-zh/products/spss-statistics</a>
Graph-Pad Prism 8 version 8.3.0 software	GraphPad	<a href="https://www.graphpad.com/features">https://www.graphpad.com/features</a>
R software (4.1.2)	R	<a href="https://cran.r-project.org/bin/windows/base/old/4.1.2/">https://cran.r-project.org/bin/windows/base/old/4.1.2/</a>

**RESOURCE AVAILABILITY**

**Lead contact**

Requests for further information should be directed to and will be fulfilled by the lead contact, Mian He ([hemian@mail.sysu.edu.cn](mailto:hemian@mail.sysu.edu.cn) & [mianhe64@163.com](mailto:mianhe64@163.com)).

**Materials availability**

All unique/stable reagents generated in this study are available from the [lead contact](#) with a completed Materials Transfer Agreement.

**Data and code availability**

- The RNA-seq data on TBLR1-overexpressed and control HeLa cells of ZXDC had been deposited to GEO: GSE234087. The Chip-seq data has been deposited to the National Center for Biotechnology Information Sequence Read Archive (SRA): PRJNA978350.
- All original code is available in this paper's [supplemental information](#).
- Any additional information required to reanalyze the data reported in this paper is available from the [lead contact](#) upon request.

## EXPERIMENT MODEL AND STUDY PARTICIPANT DETAILS

### Cell lines

We purchased the human cervical cancer cell lines SiHa, HeLa from American Type Culture Collection (ATCC, MD, USA) and kept them in our laboratory. Cell lines were authenticated by short tandem repeat (STR) fingerprinting. All the cell lines were cultured in RPMI-1640 medium (Gibco, Grand Island, NY, USA), which consisted of 10% fetal bovine serum and 1% antibiotics and then stored in a 5% CO<sub>2</sub>-humidified atmosphere at 37.0°C.

### Patients and tissues

In the present study, we collected the 118 female patients with cervical cancer who had accepted radical hysterectomy and lymphadenectomy at the Sun Yat-sen university cancer center. All the patients were diagnosed at stage IA2-IIA and underwent standard treatment from January 2007 to December 2008. Patients who had received neoadjuvant radiotherapy and chemotherapy before surgery were excluded. Survival time was calculated from the day diagnosed to the day of death, or the deadline of final follow-up. All the patients in the cervical cancer cohort had followed up more than 5 years.

Ten fresh normal samples from participants who underwent a simple hysterectomy because of hysteromyoma and had a negative-HPV status. Eight fresh cervical cancer with negative or positive lymph node metastases were collected from the first affiliated hospital of Sun Yat-sen university. All the cervical cancer patients had an HPV-positive status. We have acquired the consent of patients for the usage of their clinical material and the approval from the Institutional Research Ethics Board. The clinical characteristics of cervical cancer cohort (including age, stage, survival data, etc.) were shown in the [Table S1](#). The patients involved in our study are all Chinese, belonging to the Asian race.

### Xenograft mouse model

SCID (severe combined immunodeficiency) mice (Female, 4–5 weeks old, 18–20g) were purchased and raised in barrier facilities on a 12 h light/dark cycle. The animal experimental procedures were all approved by The Institutional Animal Care and Use Committee of Sun Yat-sen University. Briefly, mice were randomly divided into 4 groups ( $n = 6/\text{group}$ ). The stable cells ( $5 \times 10^6$ ) including ZXDC vector, scramble, ZXDC, ZXDC-shRNA#1 transduced SiHa were injected at right footpad of specific mice, respectively. After 6 weeks of inoculation, all mice were euthanized. For metastasis analysis, we measured and calculated the volumes of inguinal lymph nodes (LNs), then compared them according to grouping. Quantitative real-time PCR (qRT-PCR) analysis of hCK16 and mGAPDH can finally represent the proportion of metastasis cervical cancer cells in LNs.

## METHOD DETAILS

### Bioinformatic analysis

To further investigate the expression of ZXDC in cervical cancer, we obtained expression profiling and clinical information from three dataset of Gene Expression Omnibus (GEO, <https://www.ncbi.nlm.nih.gov/geo/>): GSE7803,<sup>31</sup> GSE67522<sup>32</sup> and GSE26511.<sup>33</sup> The GSE7803 dataset contained 10 normal squamous cervical epithelia samples and 21 invasive squamous cell carcinomas of the cervix from different patients. The GSE67522 dataset had 20 normal cervical tissue and 22 cervical cancer tissue samples from patients. Lastly, GSE26511 included 19 cervical cancer patients with positive lymph node metastasis and 20 patients without metastasis. We analyzed the expression of ZXDC in different groups within these datasets.

### Immunohistochemistry (IHC)

In brief, paraffin-embedded specimens were cut into 4- $\mu\text{m}$  sections and baked at 65°C for 30 min. The sections were deparaffinized with xylenes and rehydrated. The sections were deparaffinized with xylenes and rehydrated. Then sections submerging into EDTA antigenic retrieval buffer were microwaved for antigenic retrieval. After retrieval, tissue sections were processed with 3% hydrogen peroxide in methanol to quench the endogenous peroxidase activity, followed by incubation with 1% bovine serum albumin to block nonspecific binding, and then incubated with primary antibodies overnight at 4 °C. After washing, the samples were treated with a biotinylated anti-rabbit secondary antibody (Abcam, Cambridge, UK), followed by further incubation with streptavidin–horseradish peroxidase complex (Zsbio, BJ, China). After that, the tissues were immersed in 3-amino-9-ethyl carbazole and counterstained with 10% Mayer's hematoxylin, dehydrated, and mounted in Crystal Mount.

The specificity of the primary anti-ZXDC antibody (Proteintech, 20530-1-AP) was validated before use. The primary antibody was replaced with normal rabbit serum by coincubation at 4°C overnight preceding the IHC staining procedure for negative controls.

IHC staining was conducted on the 119 paraffin-embedded cervical cancer tissue samples using an anti-ZXDC (1:800, Proteintech, 20530-1-AP) as previously described. As for analysis, two independent pathologists who were blinded to the patients' clinical characteristics evaluated the staining results basing on the proportion and intensity of positive tumor cells. A third independent investigator would decide on the final results when there was a disagreement.

The criterial of proportion was as follows: 0, no positive cells; 1, <10% positive cells; 2, 10%–35% positive cells; 3, 35%–75% positive cells; 4, >75% positive cells. The intensity of staining was graded according to the following standard: 0, no staining; 1, weak staining (light yellow); 2, moderate staining (yellow brown); 3, strong staining (brown). The final staining index (SI) was calculated according to the following formula: SI = the proportion of positive tumor cells × the intensity. Therefore, the possible scores of SI were 0, 1, 2, 3, 4, 6, 8, 9, and 12 based on this calculating method. The cut-off value was obtained by combining the sensitivity and specificity concerning survival of cervical cancer cohort. SI ≥ 6 was applied to defined tumors with high ZXDC expression. The detailed protocol for the IHC method is provided in the [supplementary information](#) of the study.

### RNA isolation and quantitative real-time PCR (qRT-PCR)

Total RNA from cultured cells was extracted by using the Trizol reagent (Invitrogen, Carlsbad, CA, USA) as the manufacturer instructed. Subcellular RNA was isolated with the RNA Subcellular Isolation Kit (Active Motif, Carlsbad, CA, USA) according to the instructions. Reverse transcription was conducted on the different samples' RNA to form cDNA. The retrieved RNA was reverse-transcribed using M-MLV Reverse Transcriptase and amplified on a CFX384 Real-Time System (Bio-Rad Laboratories, Hercules, CA, USA). In the PCR amplification procedure, an initial amplification step using designed primers was performed with 10-min-long denaturation at 95°C and then 28 denaturation cycles at 95°C for 60 s, primer annealing at 58°C for 30 s and a primer extension phase at 72°C for 30 s. After the cycling steps, a final extension step at 72°C for 5 min was performed before the reaction mixture was stored at 4°C. The expression data were normalized by the expression level of GAPDH. The relative expression levels were normalized to the house-keeping gene GAPDH and calculated as  $2^{-(Ct \text{ of gene}) - (Ct \text{ of GAPDH})}$ , in which Ct represents the cycle threshold for each transcript. Primers used in qRT-PCR are listed below.

For the examination of half-lives of mRNAs, cells were treated with the RNA polymerase II inhibitor Act D, and RNA was isolated at the indicated time points. The half-lives of mRNAs were calculated by analyzing the relative expression levels of mRNAs normalized to untreated cells at each time point.

### Western blot analysis

Western blot analyses were performed according to a standard protocol using primary antibodies, including anti-ZXDC (Proteintech, 20503-1-AP, 1:800), anti-RhoA (Cell Signaling Technology, #2117, 1:1000), anti-ROCK1 (Cell Signaling Technology, #4035, 1:1000), anti-ROCK2 (Cell Signaling Technology, #8236, 1:1000), anti-IGF2BP3 (Proteintech, 14642-1-AP, 1:2000), anti-p-CofilinS3 (Cell Signaling Technology, #3313, 1:1000), antiCofilin (Cell Signaling Technology, #5175, 1:2000), anti-p-MLC2S19 (Cell Signaling Technology, #3671, 1:500), and anti-MLC2 (Cell Signaling Technology, # 8505, 1:1000) antibodies. GAPDH (Cell Signaling Technology, #5174) and  $\alpha$ -Tubulin (Sigma-Aldrich, T9026) were used as loading controls.

### Immunofluorescence staining of F-actin and filopodia counting

Briefly, Cells ( $5 \times 10^4$ ) were seeded on coverslips. Next day after cells reaching to 80% confluency, fixed cells with 4% PFA for 15 min at room temperature or 4°C and then rinsed cells three times with PBS. Permeabilized cells with 0.1% Triton X-100 in PBS for 10 min at room temperature. Then the cells were added 100  $\mu$ L diluent (Alexa Fluor 488 Phalloidin diluted 1:20 in PBS), incubated in the dark for 15 min at room temperature followed. Rinsed cells with PBS to remove unbound phalloidin. After that, cells were stained with DAPI (Sigma-Aldrich, St. Louis, MO, USA) which can be help to visualize and localize the nuclei. Washed cells with PBS and mounted cells with mounting medium.

The slides were viewed using a fluorescence microscope. The number of filopodia per cell as determined by actin fiber staining was calculated by counting at least 10 randomly selected cells in each exposure category.<sup>34</sup> After filopodia counting, two-sided Student's *t* test was performed to determine whether there was a statistically significant difference.<sup>34</sup> Besides, we used ImageJ to analyze the density of F-actin.

### F-actin quantification

As mentioned previously,<sup>35</sup> for each cell line, 10 conjugates from three independent experiments were analyzed for actin cytoskeleton accumulation. To quantify actin filament enrichment, we analyze the density on long axis of each cell. Fluorescence intensity of cells was measured using the Plot Profile tool of ImageJ software. Results were represented as Mean  $\pm$  SD.

### Luciferase reporter assays

In this study, we performed *RhoA* and *IGF2BP3* promoter-luciferase reporter assays to examine the role of *ZXDC* on *RhoA* and *IGF2BP3* transcription. Briefly, 20,000 cells were seeded in triplicate in 48-well plates and allowed to settle for 24 h. One hundred nanograms of reporter plasmid, plus 1 ng of pRL-TK Renilla plasmid (Promega, Madison, WI, USA), was transfected into cells using the Lipofectamine 3000 reagent according to the manufacturer's recommendation. Luciferase and Renilla signals were measured 24 h after transfection using the Dual-Luciferase Reporter Assay Kit (Promega, Madison, WI, USA) according to a protocol provided by the manufacturer. Relative luciferase activity was calculated as the ratio of luciferase to Renilla signal.

### RhoA activity assay

According to the provider's recommendations, cells were washed twice using PBS and protein was collected using cell lysis buffer supplemented 1 $\times$  protease inhibitor cocktail in the Active Rho Detection Kit (Cell Signaling Technology, Danvers, MA, USA). After centrifuging at 10000 rpm for 5 min, protein then was incubated with Rhotekin-RBD affinity beads at 4°C for 1 h. Bound proteins were washed by SDS sample buffer and then Western blot analysis was carried out according to the previously mentioned protocol.

### RNA IP (RIP) assays

In this study, RIP assays were applied to recover interactions between the proteins and mRNAs in cervical cancer cells. Briefly, cells were starved for 24 h at first and then stimulated with a standard culturing medium containing 10% FBS to initiate robust gene transcription. And then cells were harvested 8 h later and lysed in the lysis buffer (20 mM Tris-Cl, pH 8.0, 10 mM NaCl, 1 mM EDTA, 0.5% NP-40) supplemented with RNasin (Promega, Madison, WI, USA). Lysates were then pulldown with anti-*IGF2BP3* antibody (Proteintech, 14642-1-AP, 1:100) washed five times with the lysis buffer. Four different samples were designed in this part, including pulldown/IgG, Input/IgG, pulldown/IgG and Input/IgG. The retrieved pellets were then subjected to RT-PCR analysis using the RT-PCR primers of *RhoA*. *ACTB* was used as a negative control. Input serves as a positive control and was also used to normalize RNA amounts to eliminate the bias caused by different cell numbers to start with. Finally, fold changes of %Input-RNA that pulldown by anti-*IGF2BP3* were calculated by comparing to the anti-IgG group. Primers were provided in the following primary part.

### DNA constructs and establishment of stable cell lines

We performed both knockdown and overexpression of *ZXDC* on both SiHa and HeLa cells. For overexpression, the PLV/*ZXDC*-overexpression plasmid was established by subcloning *ZXDC* coding sequence into the PLV-puro vector. And for knockdown, two short hairpin RNA (shRNA) oligonucleotides were inserted into pSuper-retro-puro to generate pSuper-retro-puro-neo-*ZXDC*-shRNA (1, 2). The targeting sequences of the shRNAs were as follows.

Stable cell lines were generated from cell pools by retroviral infection. Briefly, the retroviral vectors were cotransfected with packaging plasmid into 293T cells. Viral infections had lasted for 3 days using the supernatant which contained the virus. Stable cell lines expressing *ZXDC* or *ZXDC*-shRNA were selected for 10 days with 0.5 mg/mL puromycin 48 h after infection.

### Chromatin immunoprecipitation (ChIP) assay

ChIP assay kit (SimpleChIP Enzymatic Chromatin IP Kit (Agarose Beads) #9002) was used to performed ChIP assays according to product specific protocol. Cells were first treated with 1% formaldehyde to cross-link proteins to DNA. The lysates were then sonicated and sheared to a 300–1000 bp range. Then different groups with equal amounts of chromatin supernatants were immunoprecipitated with either 1  $\mu$ g anti-ZXDC antibody (Proteintech, 20503-1-AP) or 1  $\mu$ g normal IgG antibody as a negative control, at 4°C overnight. Cross-linking of Protein-DNA complexes was further reversed, and DNA was purified. The enrichment of indicated proteins in ILF2 promoter was evaluated by qRT-PCR. Amplification of the non-promoter region was used as a negative control. Primers were provided below.

### Wound healing assay

Scratch assay was applied to measure migration and motility of cancer cells. Briefly, cells were cultured in six-well plates and formed a confluent monolayer. A sterile pipette tip was used to damage part of the confluent layer of cells, thus creating a cell-free liner “wound” in which cells can migrate. Captured the images at the beginning (0 h) and at 48 h during cell migration to close the wound, then compared the images to quantify the migrate rate of cells. The result was represented by wound closure, which calculated as the percentage of migration area relative to the initial wound area.

### Transwell migration assay

6 × 10<sup>4</sup> cells were seeded on top of the filter membrane in a transwell insert and cultured at 37°C and 5% CO<sub>2</sub> for 24 h. After that, use cotton swabs as many times as needed to carefully remove remaining cells inside the upper chamber without damaging it. Meanwhile, cells that had migrated to the bottom surface of the membrane were fixed in 1% of paraformaldehyde, stained with crystal violet. Viewed underneath an inverted microscope and counted the number of cells in three random fields of per well.

### Primers and oligonucleotides

#### Primers for qRT-PCR

hGAPDH, forward primer, 5'-GTCTCCTCTGACTTCAACAGCG-3'; reverse primer, 5'-ACCACCCTGTTGCTGTAGCCAA-3'; product size, 131 bp.

hZXDC, forward primer, 5'-AGGATGTGGGTGCTCCGAAAAG-3'; reverse primer, 5'-CGGAGCTTCTAGCTGAGGTAAG-3'; product size, 137 bp.

hKRT17, forward primer, 5'-ATCCTGCTGGATGTGAAGACGC-3'; reverse primer, 5'-TCCACAATGGTACGCACCTGAC-3'; product size, 134 bp.

hRHOA, forward primer, 5'-TCTGTCCCAACGTGCCCATCAT-3'; reverse primer, 5'-CTGCCCTTCTCAGGTTTACCG-3'; product size, 118 bp.

hACTB, forward primer, 5'-CACCATTGGCAATGAGCGGTTC-3'; reverse primer, 5'-AGGTCTTTGCGGATGTCCACGT-3'; product size, 135 bp.

hIGF2BP3, forward primer, 5'-TCGTGACCAGACACCTGATGAG-3'; reverse primer, 5'-GGTGCTGCTTTACCTGAGTCAG-3'; product size, 119 bp.

mGAPDH, 5'-CATCACTGCCACCCAGAAGACTG-3'; reverse primer, 5'-ATGCCAGTGAGCTTCCCGTT-CAG-3'; product size, 153 bp.

#### Primers for ChIP assays

ZXDC promoter region, forward primer, 5'-GGACGACAAACCTGAAGC-3'; reverse primer, 5'-CTGGCGGATAGAGGGAGA-3'; product size, 93 bp.

non-Promoter region, forward primer, 5'-GAAGGCTGTGGGAGATGA-3'; reverse primer, 5'-CCGATGACCATTAGAGGG-3'; product size, 119 bp.

*Gene silencing oligonucleotides*

ZXDC-shRNA#1:

5'-GCAGTCTGTACATTCACTCTATTCAAGAGATAGAGTGAATGTACAGACTGC-3'; ZXDC-shRNA#2:

5'-TGACGATGACCGGAGGTTTACTTCAAGAGAGTAAACCTCCGGTCATCGTCA-3'

**QUANTIFICATION AND STATISTICAL ANALYSIS**

Statistical analyses were performed using the SPSS version 19.0 statistical software package and GraphPad Prism 8 version 8.3.0 software (GraphPad software, La Jolla, CA, USA). Statistical tests for data analysis included  $\chi^2$  test (two-sided), and Student's *t* test (two-sided). Multivariate statistical analysis was performed using a Cox regression model. Survival analysis and survival curve were performed using Survival package basing on R software (4.1.2).  $p < 0.05$  was considered as statistically significant. \* $p < 0.05$ ; \*\* $p < 0.01$ ; \*\*\* $p < 0.001$ , ns, not significant.